Combust. Sci. Technol., 185: 484–513, 2013
Published with license by Taylor & Francis
ISSN: 0010-2202 print/1563-521X online
DOI: 10.1080/00102202.2012.728650

AN ANALYSIS OF THE COMBUSTION BEHAVIOR OF ETHANOL, BUTANOL, *ISO*-OCTANE, GASOLINE, AND METHANE IN A DIRECT-INJECTION SPARK-IGNITION RESEARCH ENGINE

J. Serras-Pereira,[1] P. G. Aleiferis,[1] and D. Richardson[2]
[1]*Department of Mechanical Engineering, University College London, London, UK*
[2]*Jaguar Advanced Powertrain Engineering, Coventry, UK*

Future automotive fuels are expected to contain significant quantities of bio-components. This poses a great challenge to the designers of novel low-CO_2 internal combustion engines because biofuels have very different properties to those of most typical hydrocarbons. The current article presents results of firing a direct-injection spark-ignition optical research engine on ethanol and butanol and comparing those to data obtained with gasoline and iso-octane. A multihole injector, located centrally in the combustion chamber, was used with all fuels. Methane was also employed by injecting it into the inlet plenum to provide a benchmark case for well-mixed "homogeneous" charge preparation. The study covered stoichiometric and lean mixtures ($\lambda = 1.0$ and $\lambda = 1.2$), various spark advances (30–50° CA), a range of engine temperatures (20–90° C), and diverse injection strategies (single and "split" triple). In-cylinder gas sampling at the spark-plug location and at a location on the pent-roof wall was also carried out using a fast flame ionization detector to measure the equivalence ratio of the in-cylinder charge and identify the degree of stratification. Combustion imaging was performed through a full-bore optical piston to study the effect of injection strategy on late burning associated with fuel spray wall impingement. Combustion with single injection was fastest for ethanol throughout 20–90° C, but butanol and methane were just as fast at 90° C; iso-octane was the slowest and gasoline was between iso-octane and the alcohols. At 20° C, λ at the spark plug location was 0.96–1.09, with gasoline exhibiting the largest and iso-octane the lowest value. Ethanol showed the lowest degree of stratification and butanol the largest. At 90° C, stratification was lower for most fuels, with butanol showing the largest effect. The work output with triple injection was marginally higher for the alcohols and lower for iso-octane and gasoline (than with single injection), but combustion stability was worse for all fuels. Triple injection produced a lower degree of stratification, with leaner λ at the spark plug than single injection. Combustion imaging showed much less luminous late burning with tripe injection. In terms of combustion stability, the alcohols were more robust to changes in fueling ($\lambda = 1.2$) than the liquid hydrocarbons.

Keywords: Butanol; Combustion; Ethanol; Gasoline; *Iso*-octane; Methane

Received 21 July 2012; revised 3 September 2012; accepted 6 September 2012.

Address correspondence to P. G. Aleiferis, Department of Mechanical Engineering, University College London, Torrington Place, London WC1E 7JE, UK. E-mail: p.aleiferis@ucl.ac.uk

INTRODUCTION

Understanding the effect of new bio-components on engine combustion processes is an essential challenge toward adoption of future fuel stocks that are predicted to contain a significant bio-derived component in order to promote sustainability and reduce CO_2 emissions. Ethanol can be produced from a variety of biosources and can raise the octane rating of gasoline due to its better anti-knock characteristics, allowing the use of higher compression ratios to achieve higher engine thermal efficiencies. Gasoline already contains 5% ethanol (E5) in some countries and is compatible with existing combustion systems, but its use will have only limited impact on CO_2 emissions. Therefore, there is pressure for the ethanol content of fuels to increase, with some markets demanding much higher proportions (E85 or E100). However, not all components on the current fleets of vehicles are compatible with blends containing large amounts of ethanol. Ethanol's water solubility also poses the need for rigorous procedures in its distribution and use. Furthermore, ethanol's high latent heat of evaporation can cause problems for cold engine starts due to excessive charge cooling and resulting poor evaporation. At the other end, in hot climates when used in its pure form, ethanol can also result in adverse effects such as vapor lock; blending effects can also displace light fuel fractions such as butanes. Other alkyl alcohols, such as butanol, have also been suggested as possible gasoline components. Having twice as many carbon atoms as ethanol, butanol is more hydrocarbon-like in its properties. However, butanol lags far behind ethanol in terms of commercial production.

Considering the immediate need for fundamental understanding of in-cylinder processes with bio-alcohols, no major work has been published that demonstrates direct comparisons between data obtained with ethanol, butanol, and typical hydrocarbons in modern geometry direct injection spark ignition (DISI) engines, particularly under the same operating conditions and with identical fueling systems. Similarly, the effect of modern multiple injection strategies on combustion has not been reported in the literature for ethanol and butanol fuels, although various strategies have the potential to deal with the peculiarities of the atomization process of both those alcohols that stem from their viscosity and surface tension characteristics. The following paragraphs attempt to review the literature on the subject in order to provide firm grounds for the contribution of the current article.

Combustion studies with ethanol have been mainly carried out in older generation port fuel injection (PFI) spark ignition engines. For example the studies of Brinkman (1981), Gautam and Martin (2000), Davis and Heil (2000), Al-Farayedhi et al. (2004), Nakata et al. (2006), and Topgül et al. (2006) focused on performance characteristics, while the works of Guerrieri et al. (1995), Gautam et al. (2000), Sandiquist et al. (2001), and Martinez and Ganji (2006) on exhaust emission measurements. Similarly, the combustion of butanol/gasoline blends with PFI was investigated by Alasfour (1997) and Swaja and Naber (2010) in single-cylinder research engines. In an attempt to bridge the gap of our understanding between PFI and direct injection (DI) of alcohols, Zhu et al. (2008) reported on the combustion characteristics of ethanol on a single cylinder dual-fuel injection spark ignition (SI) engine with the following fueling cases: (a) gasoline PFI and DI, (b) gasoline PFI and ethanol DI, and (c) ethanol PFI and gasoline DI. In their study, the DI fueling

portion varied from 0–100% of the total fueling over different engine conditions, while the engine air-to-fuel ratio remained constant. It was shown in all cases that the indicated mean effective pressure (IMEP) decreased by as much as 11% as DI fueling percentages increased, except in case (b) where the IMEP increased by 2% at light load. The combustion burn duration increased significantly at light load as DI fueling percentage increased, but only moderately at wide open throttle (WOT). In addition, the percentage of the ethanol in the total fueling played a dominant role in affecting the combustion characteristics at light load; but at heavy load (WOT), the DI fueling percentage became the important parameter, regardless of the percentage of ethanol in the fuel. These results do not necessarily agree with those of Aleiferis et al. (2008), which showed that direct injection increased the speed of mass fraction burned in general with both gasoline and gasoline/ethanol blends. One reason for this discrepancy might be that Zhu et al. (2008) used a low pressure multihole side injector at an angle of 35° from the horizontal with a nine-hole orifice plate and a spray angle of 60° (at 20 bar) compared to the pressure-swirl injector at 80 bar used in the study of Aleiferis et al. (2008). Although both injectors in these two studies were side-mounted, the higher injection pressure used in the latter study would not only improve atomization significantly but would also reduce dramatically the injection pulse-width; these factors would contribute to a better mixture preparation than obtained by the system used in Zhu et al. (2008). This example illustrates that results should not be assumed to carry over easily to various combustion systems, and that there are difficulties in drawing general conclusions from such data in the literature, when changes in hardware and operating strategies can easily change the outcome of a particular test in practice. Other recent studies with various types of injection systems for DISI engines presented results with a diversity of gasoline/ethanol and gasoline/butanol blends but did not focus on comparing pure ethanol and butanol fuels (Aleiferis et al., 2010b; Brewster, 2007; Cairns et al., 2009; Kapus et al., 2007; Wallner et al., 2009). The optical studies of Serras-Pereira et al. (2008) with ethanol and butanol DI, using early injection for homogeneous engine operation, as well as that of Smith and Sick (2007) with ethanol and *iso*-butanol DI, using late injection for stratified operation, provided some useful insights, but did not focus on various fuel types and strategies over a large area of low-load engine conditions.

PRESENT CONTRIBUTION

There are very limited experimental data that clarify the role that liquid transport properties have on mixture formation and combustion over a realistic range of DISI engine operating conditions. The main objective of the current work has been to study the combustion process of ethanol and butanol fuels versus gasoline and *iso*-octane operation in the context of advanced injection strategies that promote better mixture formation and in direct comparison to the gaseous fuel, methane. Specifically, a comprehensive study was undertaken to provide robust performance data of the fuels' sensitivity to different operating conditions (stoichiometric and lean).

Planar laser induced fluorescence (LIF) in the same engine has provided imaging of the fuel's concentration during mixture formation with a specially designed model fuel (Williams et al., 2008). Considering the importance of the in-cylinder

air-to-fuel ratio (AFR) at the spark plug location at ignition timing for all fuels, further LIF was considered. However, due to issues of quantification of the fuel concentration by LIF with such a diverse range of fuel and engine operating conditions, e.g., stemming from fluorescence quenching at different rates by the base fuels (Smith and Sick, 2007), it was decided to use in-situ fast flame ionization detection (FFID) to measure the value of the mixture's equivalence ratio at ignition timing. Specifically, mixture preparation was studied by FFID at the spark plug location and the liner wall in order to investigate the degree of charge stratification.

To the best of the authors' knowledge, this is the first time that such a complete set of data is presented for ethanol and butanol in direct comparison to typical hydrocarbons fuels in a latest geometry SI combustion system. It is believed that these measurements contribute to a database of combustion rates that are essential for developing our knowledge of the underlying fundamental mechanisms of biofuel behavior under realistic engine conditions. The data can also assist modelers because the simulation of mixture preparation and combustion with fuels of such diverse physical and chemical properties is still very challenging.

EXPERIMENTAL APPARATUS AND PROCEDURES

Research Engine

A single-cylinder research engine was used to investigate for this study. The engine is based on a flexible modular design for thermal or optical in-cylinder studies, provided by Ford Research Laboratories (Dearborn, MI, USA). The current work employed a Jaguar four-valve engine head based on a cylinder of a V8 4.5 L prototype four-stroke DISI engine, with a vertical and centrally mounted multihole direct-injection system in a close-spacing arrangement with the spark-plug; the spark-plug was inclined at $\sim 15^{\circ}$ from vertical. The valvetrain was composed of double-overhead cam-shafts with direct acting lobes, and a fixed valve-timing was used throughout. The geometric parameters of the engine, as well as other system components, are summarized in Table 1, while Figure 1 shows the engine configuration. With regard to intake geometry, the engine was fitted with an "inverted-U" tumble-inducing manifold upstream of the inlet ports. The piston was of elongated Bowditch type and used three sets of lubricating rings made of Torlon (two sets of two thin rings in close spacing arrangement and a third wide bottom ring). These

Table 1 Research engine specifications

Engine base type	Prototype head
Cycle	4-Stroke
Cylinders	1
Valves	2 Intake, 2 exhaust
Bore	89.0 mm
Stroke	90.3 mm
Compression ratio	11.15:1
Valve timings	IVO 24°, IVC 274°, EVO 476°, EVC 6°

EVO – exhaust valve open; IVO – intake valve open.

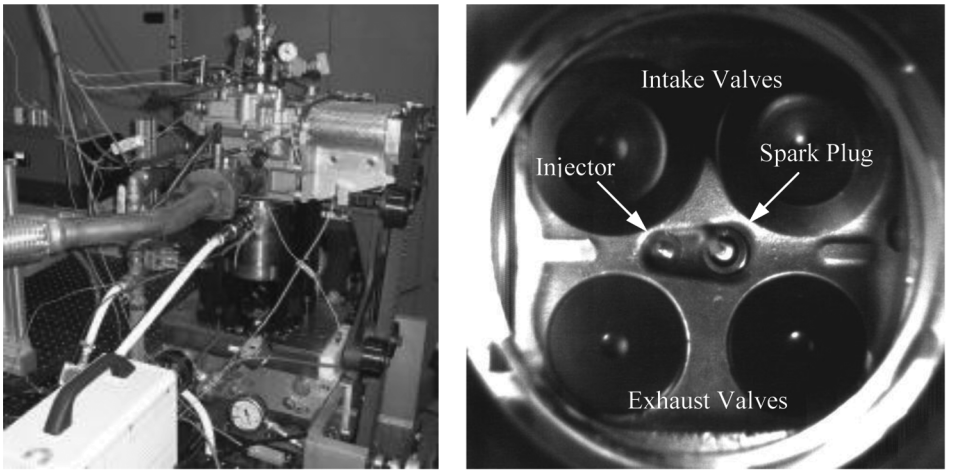

Engine on test bed Chamber view through fully optical piston crown

Figure 1 Single-cylinder research engine.

allowed us to run the cylinder liner oil-free to prevent fouling of the windows. Since the standard piston in the cylinder block (under the 45° mirror) was oil lubricated, in order to prevent oil vapor from passing through the rings and misting the 45° mirror, a vacuum network was designed from the engine head to the crank-case providing ~0.3–0.4 bar negative pressure.

For the purpose of comparing the fuels in the current article, the quartz piston crown was replaced by a metal piston crown, and the quartz liner was replaced by a water cooled metal liner. An in-house designed water system was used to circulate cooling water around the engine head and cylinder liner and incorporated a temperature control system comprising a three-way valve to divert water to a heat-exchanger and two 1.5 kW immersion heaters. A Eurotherm 3216 PID controller was used to select the temperature set-points and calibrate the temperature control dynamics. Water temperature control from 10°C (nominal engine test cell cooling water temperature) to 90°C was possible under motoring and firing conditions within a 1–2°C range. For the current work, the influence of engine temperature was observed by using engine head and liner coolant temperatures of 20°C, 50°C, and 90°C. Enough heat-soak time (30–40 min) was allowed at all conditions so that the engine head and liner components acquired enough thermal inertia to simulate fully warmed-up conditions.

The ignition system used was a transistorized coil-on-plug (TCP) type driven via a 12 Volt DC, 25 A power supply, which also powered the injector driver. A commercial J-type ground electrode with a V-grooved central electrode, laser-iridium spark-plug was used (NGK IKAR6_IX9) that had a heat rating of 6 and a 0.9 mm spark gap. A charge time of ~4 ms was employed.

The ignition and injection timings were controlled using an AVL 427 engine timing unit (ETU) that generated crank-angle or time-based controlled trigger signals. A combination of ''working'' and ''waiting'' cycles could be programmed with the ETU; more than one pulse group could also be generated per cycle. These

capabilities were exploited for the FFID measurements, as will be described later. For engine synchronization, the ETU required two inputs to define a "clock" term and a "reference" signal term, i.e., the crank-degree-marker (CDM) and the top-dead-center (TDC) signals, respectively. Both signals were supplied from the output of an optical encoder on the engine's crank shaft (Leine-Linde 503), with the CDM corresponding to 1800 pulses/revolution and the TDC cycle-reference provided by a once/revolution TTL signal. The ETU used the TDC signal to reset its internal clock every crank shaft revolution in order to maintain optimum synchronization accuracy on a cycle-by-cycle basis.

The A/F ratio (AFR) was measured using a heated zirconia-based high-speed oxygen sensor (ECM AFR Recorder 1200) installed in the exhaust manifold ~150 mm along the exhaust pipe from the engine head. The sensor allowed programming of the H-C and O-C ratios in order to accommodate different hydrocarbon and alcohol fuels. The measurable AFR ranged from $\lambda = 0$–10 or 0–150 AFR easily accommodating even aggressively lean operating strategies. The sensor was calibrated for oxygen sensitivity using compressed air and N_2 gas bottles. Further details about the engine test bed arrangement can be found in previous publications by the current authors on in-cylinder spray dynamics and combustion (Aleiferis et al., 2010b; Serras-Pereira et al., 2007).

Fuels

Five fuels were investigated: a typical commercial grade gasoline [research octane number 95 (RON95)], *iso*-octane, *n*-butanol (1-butanol), ethanol, and methane. A standard commercial grade European gasoline contains several hundred hydrocarbons, typically about 25–30% C5 or lower, 30–40% C6–C8, and the remainder C9–C10 hydrocarbon chains. *Iso*-octane is a single component of gasoline with boiling point temperature of 99°C at atmospheric pressure, while, in contrast, butanol boils at 118°C and ethanol at 78.4°C. The distillation curve of the gasoline

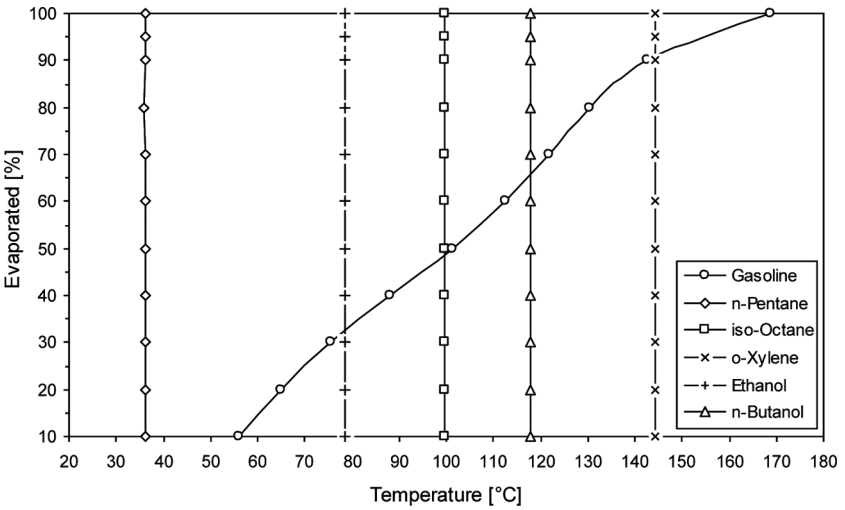

Figure 2 Distillation curve of gasoline and boiling points of single-component fuels.

fuel is shown in Figure 2. The boiling points of *iso*-octane, ethanol, and butanol at 1.0 bar are shown in Figure 2 also as vertical lines; the boiling points of the single components *n*-pentane and *o*-xylene have also been included in Figure 2 for reference purposes and in order to highlight two high and low volatility hydrocarbon components in gasoline, respectively. Table 2 summarizes the most important physical and chemical properties of all the fuels used. It needs to be noted here that, within the objectives of the current work, it was decided to test pure *n*-butanol instead of blends of it (or of other isomers, like *iso*-butanol) with gasoline and/or *iso*-octane, in an attempt to establish fundamental effects of this straight chain alcohol in direct comparison to pure ethanol, rather than warrant wide use of this fuel in pure form (since source-to-wheel energy expenditure and other issues may dictate that it is better suited to use in low-to-moderate blending levels). However, various blends of different butanol isomers with gasoline and *iso*-octane are currently also being studied and will be reported in a future publication.

Table 2 Fuel properties[a]

Properties	Ethanol	Butanol	Gasoline	*iso*-Octane
Chemical formula	C_2H_5OH	C_4H_9OH	$C_{6.75}H_{12.99}$ (C_4–C_{12})	C_8H_{18}
Molar mass [g/mol]	46.07	74.12	100–105	114.3
Density [g/cm^3]	0.79	0.81	0.72	0.69
Solubility in water (20°C) [g/l]	Miscible	79	Partially	5.6×10^{-4}
Boiling point [°C]	78.3	117.8	~55–145 (10–90%)	99
Flash point [°C]	12	30	−43	−12
Autoignition temperature [°C]	425	340	>350	410
Reid vapor pressure [kPa]	16.1[b]	2.2[b]	56	11.8[b]
Dynamic viscosity (20°C) [cP]	1.2	2.95	0.37–0.44[c]	0.51
Dynamic viscosity (80°C) [cP]	0.43[d]	0.73[d]	–	0.27[d]
Kinematic viscosity (25°C) [cSt]	1.34[d]	3.22[d]	0.5–0.58	0.67[d]
Kinematic viscosity (80°C) [cSt]	0.59[d]	0.96[d]	–	0.42[d]
Surface tension (20°C) [mN/m]	24.05[d]	26.3[d]	~20	18.3[d]
Surface tension (80°C) [mN/m]	16.4[d]	19.3[d]	–	13.6[d]
Explosion limit (upper) [Vol%]	15	11.3	7.6	6
Explosion limit (lower) [Vol%]	3.5	1.4	1.4	1
Latent heat (T_{boil}) [kJ/kg]	855[d]	584[d]	364	272[d]
Latent heat (25°C) [kJ/kg]	874[d]	669[d]	380–500	300[d]
Stoichiometric AFR	9	11.1	14.6	15.1
Heating value [MJ/kg], [MJ/lt]	26.9, 21.3[d]	33.9, 27.5[d]	42.7, 32[c]	44.6, 30.8[d]
Specific energy [MJ/kg air]	2.99	3.01	2.92	2.94
RON	129[e]	96[e]	95	100
H/C	3	2.5	1.92	2.25
O/C	0.5	0.25	0	0

[a]If not specified differently, data taken from fuel product sheets; Scharlab (2011a, 2011b, 2011c), Shell Global Solutions (UK) (2005).
[b]Poling et al. (2001).
[c]Owen and Coley (1995).
[d]Yaws (2003).
[e]Gupta and Demirbas (2010).

Injector

A six-hole injector designed for vertical installation in a DISI engine head in close spacing arrangement with the spark plug of a gasoline engine was used for this investigation. The injector had six nozzle holes in an asymmetric arrangement with different angles with respect to the vertical axis. More details about the exact injector geometry, nozzle-hole angles, and spray formation in a quiescent environment and in a running DISI engine can be found in previous studies (Aleiferis and van Romude, 2013; Aleiferis et al., 2010a, 2011; van Romunde and Aleiferis, 2009; van Romunde et al., 2007). For all work presented in this article, the fuel pressure was maintained at constant 150 bar. Methane was injected in the intake plenum using a Keihin KN3-2 gas injector and 4 bar injection pressure. Typically, when injecting gaseous fuels with PFI, some air is displaced by the gaseous fuel, leading to an in-cylinder charge with lower total energy than if the gaseous fuel had been injected with DI after intake valve closure. Therefore, sometimes researchers elect to adjust the throttle to account for the "lost" air. Within the objectives of the current study, it was deemed necessary to keep the same intake plenum conditions for all fuels in order to keep the in-cylinder flow nominally matched to that of the other fuels because any effect of engine load on the mean flow and turbulence intensity at ignition could mask or exaggerate effects when comparing fuels. This issue was carefully considered throughout analysis of the acquired data, and more comments will be provided in the Results section.

Experimental Techniques

The experimental configuration consisted primarily of in-cylinder pressure acquisition and in-cylinder FFID measurements. Flame images were also acquired to compare two injection strategies, as will be discussed later. The baseline engine condition approximated to a well-known reference engine mapping point, known as the world wide mapping point (WWMP), producing ~2.62 bar brake mean effective pressure (BMEP) and referring to low-load, low-speed inner city driving conditions, of 1500 revolutions per minute (RPM) with 0.5 bar intake pressure. The engine valve timings at this load corresponded to levels of internal exhaust gas residuals (EGR) of the order 15%, as discussed in more detail later. The ignition timing was varied in the range 50°–30° crank angle (CA) before-compression top dead center (BTDC) to build up maps of each fuel's behavior.

The baseline injection strategy used a single injection event with timing set early in the intake stroke to promote homogeneous mixture formation, typically with start of injection (SOI) 80°CA after-intake top dead center (ATDC) and duration to fit the required AFR as observed by the lambda sensor. However, injection timings were also studied throughout a range of 60°–220° ATDC for comparison. Additionally, a multi-injection strategy with three small split injections at SOI 60°, 70°, and 80°CA (i.e., dwell time 10°CA) was also employed to assess the effect on mixture preparation and combustion. The three smaller injection TTL pulse widths were roughly each one-third duration of the single injection duration; however, this varied slightly depending on operating strategy and fuel type. The exact pulse widths used for all conditions are summarized in Table 3.

Table 3 Fuel pulsewidths used for all fuels and injection strategies

	Engine mapping fuel pulse durations [ms]		
	1.0		1.2
$\lambda = \mathrm{AFR}/\mathrm{AFR}_{\mathrm{stoich}}$ Injection strategy	Single	Triple	Single
iso-Octane	0.90	0.3, 0.3, 0.35	0.74
Gasoline	0.90	0.3, 0.3, 0.35	0.74
Ethanol	1.38	0.3, 0.4, 0.62	1.14
Butanol	1.10–1.16	0.3, 0.4, 0.45	0.91–0.96
Methane	3.90	–	3.10

In-cylinder pressure measurement and analysis. The in-cylinder pressure measurements for the present study were conducted with a water-cooled piezoelectric pressure transducer (Kistler 6041A). The sensor was installed flush with the engine pent-roof walls and was connected to a Kistler 5011B10 desktop charge amplifier. When the signal is digitized, it is necessary to define a reference datum to convert it to absolute pressures. This can be done by using another pressure transducer towards the bottom of the cylinder barrel so that when the piston is close to bottom dead center (BDC), the transducer records the absolute and thus reference in-cylinder pressure. This was done with a water-cooled piezoresistive transducer (Kistler 4075A10 sensor and Kistler 4618A0 amplifier) mounted on the side of the cylinder 75 mm below the head gasket plane. When the piston was above the barrel transducer, the pressure measured was atmospheric as a result of the "floating" cylinder design of extended piston optical engines.

The pressure signals were digitized at a sampling rate of 45 kHz on a cycle-to-cycle basis with a 12-bit analogue-to-digital converter (National Instruments PCI-MIO-16E-4). This rate corresponded to digitization every 0.2°CA. The uncertainty due to electrical interference was a maximum of 0.05% of the full scale value for the in-cylinder pressure and 1% of full scale value for the intake plenum and barrel pressures, corresponding to an uncertainty of ± 5.0 mbar and ± 10 mbar respectively. The CDM pulse from the crankshaft encoder was used via the ETU to provide the clock source for a LABVIEW-based data acquisition program. Heat release analysis of the in-cylinder traces and calculation of mass fraction burned (MFB) was performed using methods based on Ball et al. (1998) and Stone and Green-Armytage (1987). The effects of numerical integration on the calculation of the indicated mean effective pressure (IMEP) from the in-cylinder pressure-volume diagram can be minimized, provided the crank angle resolution is smaller than 1°CA (Brunt and Emtage, 1996). Errors can also arise from the effects of signal noise, accurate definition of con-rod length, and the correct phasing of TDC with pressure. These researchers reported a $\pm 2.5\%$ uncertainty in IMEP given a ± 0.5°CA uncertainty in the phasing of TDC. In the current arrangement, the accuracy of the con-rod length was accurate to below 0.01% and the position of TDC was accurate to within less than ± 0.1°CA such that errors in IMEP and mass fraction burned due to the experimental arrangement were considered to be negligible. A representative number of cycles for analysis was identified on the basis of the coefficient

of variation of IMEP (COV_{IMEP}) that achieved steady-state values at about 150–200 cycles depending on conditions, hence 200 cycles were used for each test point analysis.

In-cylinder fast-FID measurement and calibration. An HFR400 Cambustion fast-flame ionization detector (FFID) was used in order to carry out cycle-resolved hydrocarbon measurements inside the engine and in particular to investigate the degree of stratification in the mixture field at ignition timing for different fuels and injection strategies. The installation of the FFID head on the engine is shown in Figure 3. The basic design of a FFID system involves a diffusion flame of hydrogen in a slow coflowing stream of air and a sampling system that isolates the pressure fluctuations at the sampling point in order to provide a constant mass flow of the sampled gas to the detector. Negligible ionization occurs until hydrocarbon species are introduced, and the ions are then collected by a charge collector located just above the burner. The response time allows intracycle measurements. A detailed description of the sampling system and its performance was given by Cheng et al. (1998); reviews of different applications including in-cylinder sampling were also presented.

The FFID has been found to respond with proportionality to alkanes, cyclo-alkanes, alkenes, alkynes, and aromatic compounds with different number of C atoms in each molecule of these families of compounds and the linearity of the instrument means that the FID is generally conceived as a carbon counting device for hydrocarbons. The response function for other carbon containing compounds has been shown to be different however. For example, for alcohols and other compounds where carbon is already oxidized in the starting sample, an oxidized carbon fragment splits out in the endothermic cracking stage of the reactions, and this oxidized carbon fragment is incapable of producing ionization in the flame (Cheng et al., 1998). Specifically for alcohols, the C bonded to O in the alkyl-O-H group contributes only to a fraction of a C atom. This is governed by the bond rupture process, whether it occurs through the removal of the H atom (which does not produce ions)

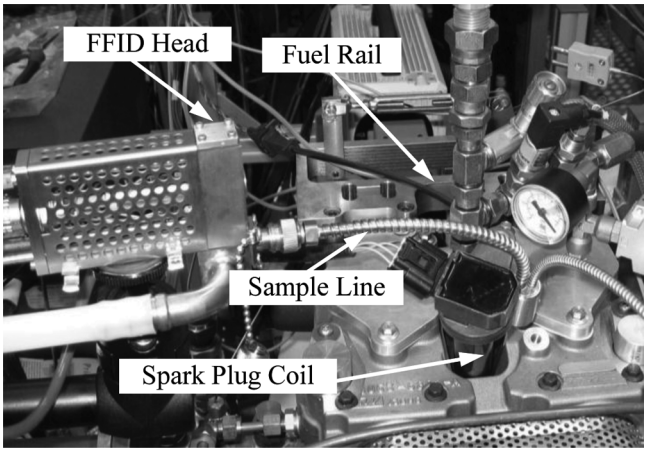

Figure 3 FFID installation on single cylinder engine for spark-plug in-cylinder measurements.

or the removal of OH (which does). The contributions of various bonds to the effective carbon number FFID response are given in Cheng et al. (1998); for primary alcohols the effective contribution was 70% for ethanol and 85% for butanol. More details can be found in recent publications (Dec et al., 2008; Price et al., 2007; Wallner, 2011; Wallner and Frazee, 2010).

The main difficulty with the FFID technique applied to in-cylinder measurements is controlling the sample mass flow rate to the FID head, which pulsates substantially as a result of the range of pressures that the sample probe is exposed to, e.g., sub-atmospheric to ~20–30 bar, for part-load engine operating conditions similar to those used in the present study. For intake and exhaust pressure measurements, a constant pressure chamber is used between the sampling inlet and the FID detector itself, operated at below atmospheric pressure to act as a damping chamber and maintain a constant pressure across the feed tube to the FID chamber; for in-cylinder measurements, however, this is not enough. The flow resistance through the sample tube needs to be reduced further by using a smaller diameter tube of 0.008 inches and the constant pressure chamber volume must be increased substantially, which can be done by opening it to atmosphere, i.e., infinite volume. One of the drawbacks from such a configuration is that positive flow to the FID head only occurs when the in-cylinder pressure is substantially above atmospheric; the engine intake valve timing therefore dictates when this begins to occur, and, given the limited response time of the FFID relative to engine speed, certain checks need to be made to make sure there is enough time for the signal to reach its plateau value every cycle.

The expected characteristics of a typical in-cylinder FFID signal are shown in Figure 4. The signal is initially low due to burned gas left over from the previous cycle; as fresh charge enters the cylinder and mixes with the residual charge, the signal rises gradually but is not yet valid due to low FFID response as a result of low sample inlet pressure. As the cylinder pressure rises during compression, the FFID response improves, and at some point the signal reaches a plateau level, which is the pre-flame hydrocarbons (HC) mole fraction. The value measured is actually less

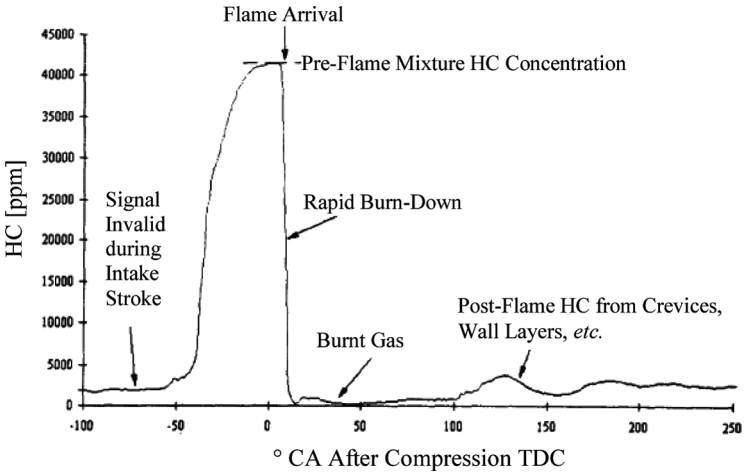

Figure 4 Typical FFID signal from in-cylinder sampling (Cambustion HFR 400 Manual).

than the equivalent air/fuel ratio mixture because the residual gas acts as a dilutant. When the in-cylinder flame arrives, there is a sharp drop in the signal, and the fall-time can be interpreted as the response time of the FFID. The signal remains low while it is exposed to burned gas, but later in the cycle the FFID detects post-flame hydrocarbons released from the crevices and the signal rises again slightly. The signature of the signal in this area depends on the location of the sample inlet, with higher values measured when the sample probe inlet is close to the walls and protrudes only slightly, ~0.1–1 mm.

The FFID response time is also adversely affected by condensation and liquid fuel in the sample tube, and a heated line was therefore used at 150°C to reduce these effects. Suitable calibration with a known concentration gas is also necessary; however, since quite high concentrations are necessary for calibration at stoichiometric conditions, the gas is usually mixed with nitrogen. Unfortunately, in real engine measurements the HC sample is mixed with air and the FFID signal is sensitive to the oxygen content in the sample flow, leading to a decreased response function (termed oxygen synergism). To overcome these effects, the engine was motored and fired at stoichiometric conditions with methane gas using intake plenum injection to provide as a homogeneous concentration field at ignition timing as possible; dynamic calibration under real operating conditions was thus achieved. This FFID signal then allowed direct comparison of the HC mole fractions obtained using other liquid fuels and estimation of relative air/fuel ratios. A spark-plug sampling kit from Cambustion was used to obtain in-cylinder samples of HC just next to the spark electrode (~1 mm). Another sampling probe was positioned in the pent-roof wall (~2 mm above the wall face) using an adaptor to fit the in-cylinder pressure transducer mounting hole and thereby investigate the stratification of the charge. The FFID settings are summarized in Table 4. The FFID signal was digitized using LABVIEW and post-processed for statistical analysis in MATLAB.

Motoring, firing, and skip-firing engine operation were used to guarantee the integrity of the FFID signals acquired. Due to the late intake valve closing, the pressures at ignition timing were quite low, ~3.5–4 bar, and the time response of the FFID was not fast enough to fully achieve a plateau signal in every cycle. Therefore, "skip-firing: was used: the engine was fired for 10 cycles and motored for 10 cycles. This was useful because a signal over a 20-cycle batch allowed a sufficient average signal to be obtained. Fifty duty-cycles of this skip-fired strategy were employed,

Table 4 FFID system configuration for in-cylinder sampling

Specifications	In-cylinder FFID
ΔP [mm Hg]	55
Fuel flow [bar]	2.2
Air flow [bar]	5.1
Calibration gas	Methane
C1 stoichiometry [ppm]	95,057
Sample probe length [mm]	330
Sample probe diameter [inches]	0.008
Sample probe locations	Spark plug and pent-roof wall
CP chamber	Open to atmosphere

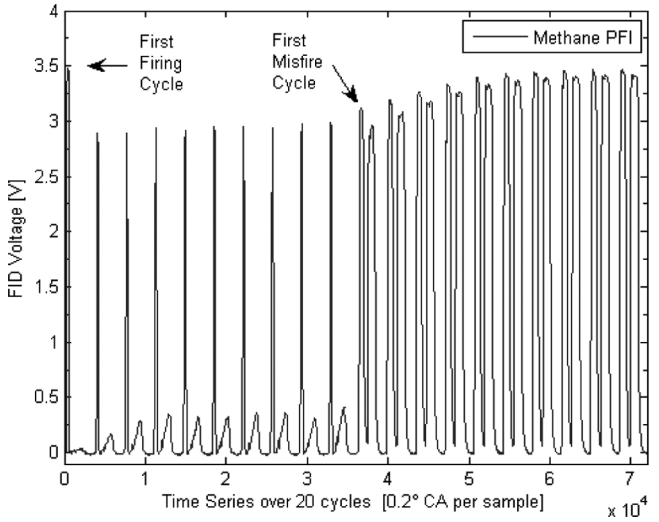

Figure 5 FFID signal with skip-firing sequence over 10 motoring and 10 firing cycles, methane (0.5 bar inlet plenum pressure, $\lambda = 1.0$).

i.e., 1000 engine cycles, and the average signal was obtained as shown in Figure 5. The data are shown for methane fueling at stoichiometric conditions. The first FFID peak identifies the first firing cycle in the sequence and shows that its value was higher than for the remaining firing cycles due to the absence of residual gas. The remainder of the cycles can be seen to be quite similar, however, demonstrating a low level of cyclic variation and indicating that a residual gas "steady state" condition was reached within one firing cycle. After the spark was switched off, the value of the peak FFID signal increased to a level that represented the mole fraction measured without residuals. The difference between these signal levels and the firing levels allowed estimation of the residual gas fraction. This was found to be ~0.15–0.2 for the conditions studied, and the values were found to be in agreement with values calculated by modeling the engine's operation using geometrical and valve timing data via the methodology offered by the Lotus Engine Simulation Software (2010). Figure 6 shows evidence of insufficient signal response time available under firing conditions and why such a skip-firing strategy was necessary to achieve a reliable FFID plateau value. The plateau level for stoichiometric methane combustion had a coefficient of variation (COV) of only 1.0% at the spark-plug and 1.7% at the wall location. Since the concentration field was as homogeneous as possible, the variation probably stemmed from variations in the residual gas fraction from cycle-to-cycle and contributions from the measurement accuracy of the instrument itself. Evidence of the sensitivity and linearity of the instrument with different air/fuel ratios is demonstrated in Figure 7 for a liquid fuel, *iso*-octane, also obtained with the skip-firing strategy outlined.

In-cylinder combustion imaging. For the purposes of the current article, it was deemed necessary to image the in-cylinder combustion event up to completion in the expansion stroke in order to identify late burning on the cylinder walls from effects related to the different injection strategies used. To achieve this, the standard

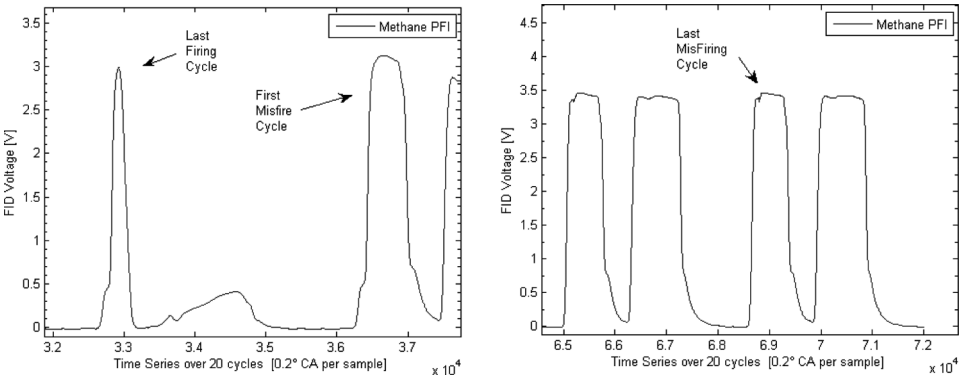

Figure 6 Magnified FFID signal in skip-firing sequence.

aluminum piston crown was replaced by a full-bore optical crown designed and made of Perspex in one piece by the University of Oxford; see Ma et al. (2007) and Aleiferis et al. (2011) for more details. The fully optical crown connected to the Bowditch piston using the same thread as the standard metal crown. This configuration extended the 65 mm diameter optical access used in previous studies, e.g., Serras-Pereira et al. (2007, 2008) and Aleiferis et al. (2010b), to 89 mm in diameter, i.e., the full bore diameter, as shown in Figure 1. Additionally, the fully optical crown was designed with a fish-eye lens configuration (by keeping the top of the crown flat and contouring the inside/lower part of crown) to allow full clear optical access up to the liner walls via a 45° mirror housed under the crown inside the Bowditch. More details about this piston arrangement as used in the same engine for spray wall impingement imaging can be found in Aleiferis et al. (2011). A high-speed

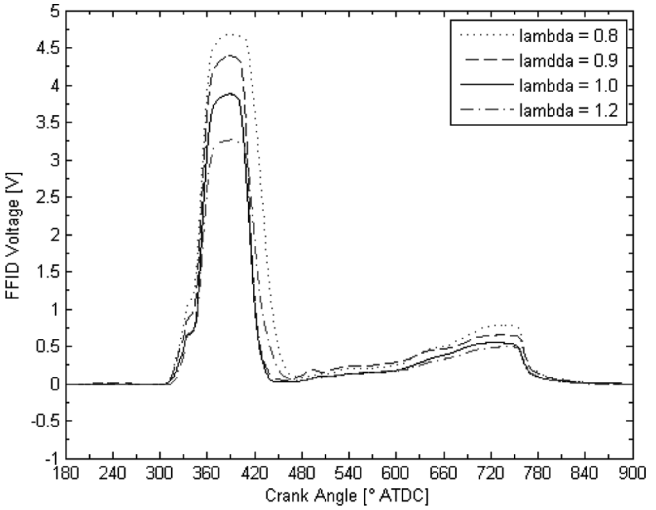

Figure 7 Average FFID signal at the spark-plug for different values of air-fuel ratio: *iso*-octane, single injection strategy with SOI 80°CA ATDC, 90°C.

camera (Photron APX-RS) was used to obtain combustion images with 640×480 pixel resolution with a typical frame rate of 9 kHz, i.e., 1°CA resolution at 1500 RPM. More details about the imaging equipment can be found in other studies by the current authors (Serras-Pereira et al., 2007, 2008). The images were stored in 8-bit resolution in tagged image file format (TIFF) files (256 grayscales). The camera was triggered externally with a pulse supplied by the ETU for synchronization with the engine and other instrumentation.

RESULTS AND DISCUSSION

Fuel Type Sensitivity

The engine's operating performance at stoichiometric conditions with single injection strategy is shown in Figure 8 for all fuels at 20°C, 50°C, and 90°C engine temperature. The measurements acquired at lean conditions with single injection strategy and at stoichiometric conditions with triple injection strategy are presented in Figures 9 and 10, respectively. The figures include the following combustion parameters: peak in-cylinder pressure (P_{max}), the timing or location of peak pressure (θ_{Pmax}, i.e., combustion phasing), the net indicated mean effective pressure ($IMEP_n$), the 0–10% MFB duration ($\chi_{b10\%}$, i.e., the early flame kernel growth period), and the 10–90% MFB duration ($\chi_{b10-90\%}$, i.e., the main combustion period). The coefficient of variation (COV) of all parameters has also been plotted within the same figures for comparison.

In-cylinder pressure and IMEP. The phasing of P_{max} can act as a measure of the efficiency of combustion when studied in conjunction with the IMEP. The cycle-to-cycle variations in P_{max} and IMEP are typically used as a measure of the stability of combustion. Additionally, the amplitude of P_{max} and its phasing can be used as a relative measure of the propensity toward "knocking" combustion when changing spark advance. In general, the sensitivity of the combustion process to ignition advance was similar for most fuels in terms of P_{max} and phasing of P_{max}; this is seen by the similar gradients of the trend lines in Figure 8. However, the absolute values of P_{max} and the phasing of P_{max} were both clearly different among fuels; there appeared to be a distinct performance hierarchy that was almost independent of engine operating temperature. This was also reflected in the COV_{Pmax}. For all fuels tested, greater ignition advance resulted in higher P_{max} and lower cycle-to-cycle variations (COV_{Pmax}). Similarly, higher engine temperatures generally resulted in higher pressures and lower levels of variation across the range of ignition timings that were tested. At 20°C engine temperature, the highest levels of P_{max} were recorded for ethanol, methane, butanol, gasoline, and *iso*-octane, respectively. It needs to be noted, though, that butanol was difficult to ignite at these conditions, and the engine required a period of ~1 min in order to ignite consistently and stabilize in operation. The largest difference in P_{max} between ethanol and *iso*-octane was recorded at 40°CA spark advance and was ~5 bar in magnitude. Ethanol's P_{max} was also ~5°CA advanced relative to TDC. The fuel hierarchy was inverted for the COV_{Pmax} and IMEP. Ethanol exhibited the lowest values of COV_{Pmax} (~5% at the largest spark advance) and *iso*-octane the highest (about 10–13% over the full range of tested ignition timings).

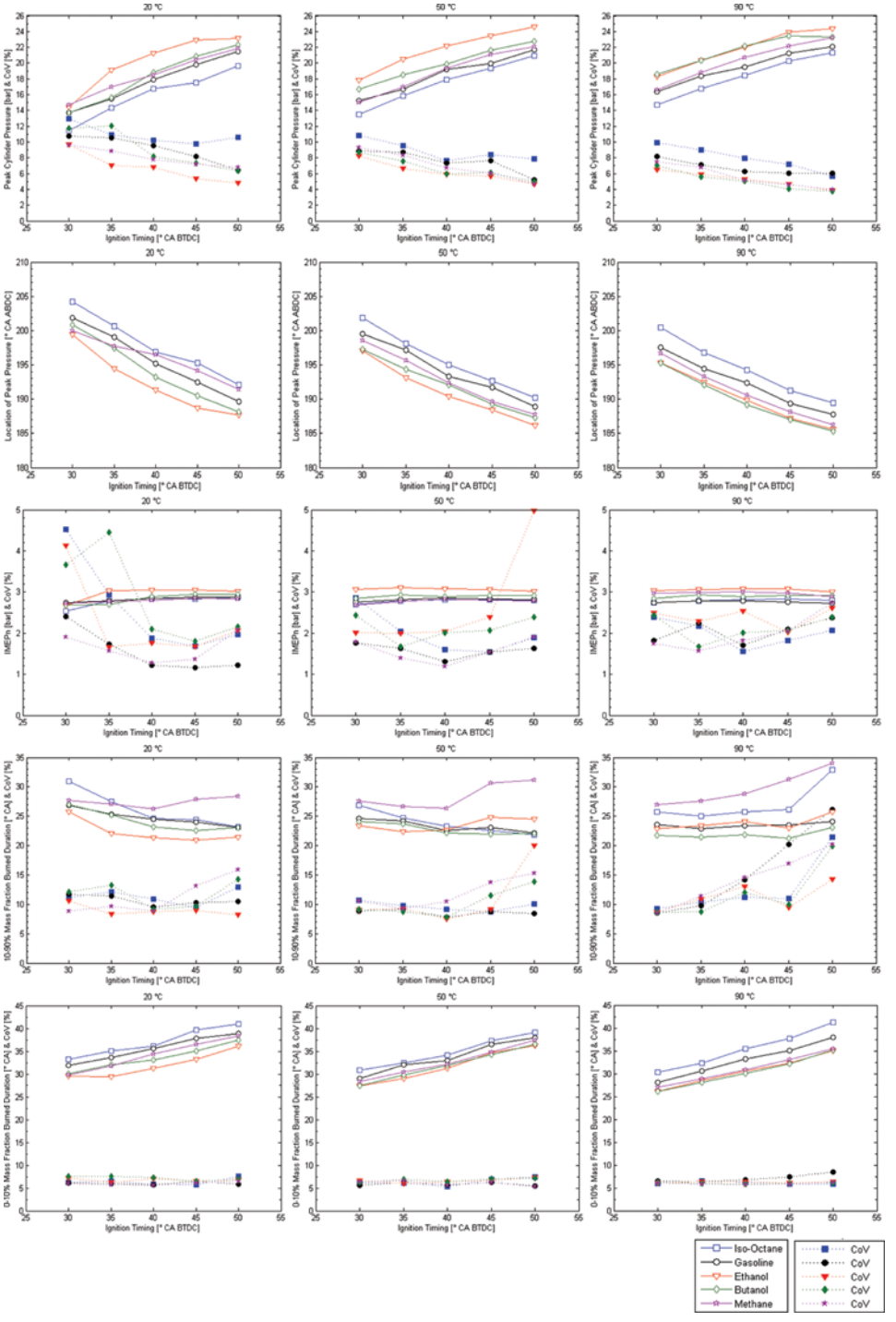

Figure 8 Combustion performance with single injection strategy at 20°C, 50°C, and 90°C; all fuels ($\lambda = 1.0$). (Figure is provided in color online.)

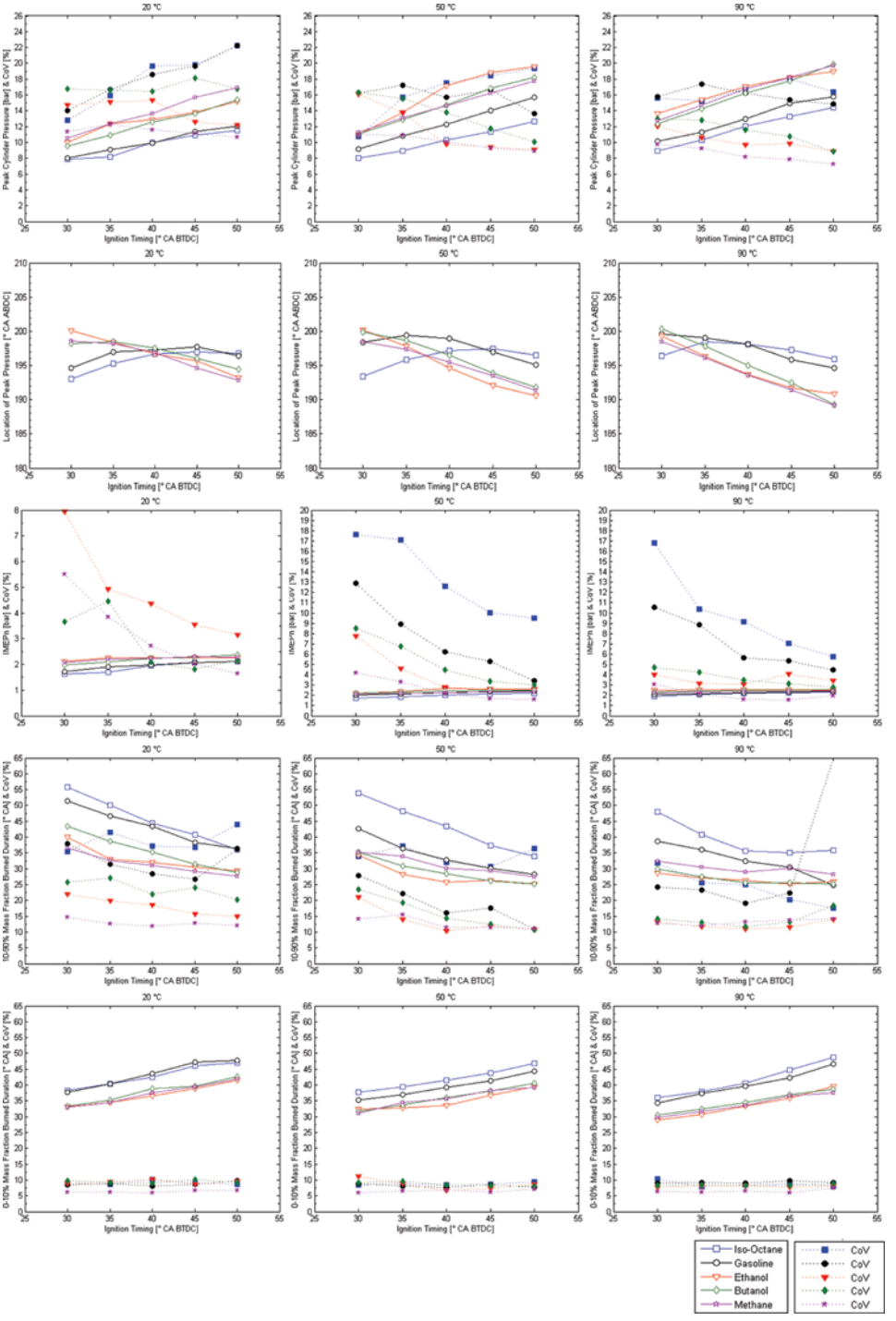

Figure 9 Combustion performance with single injection strategy at 20°C, 50°C, 90°C; all fuels ($\lambda = 1.2$). (Figure is provided in color online.)

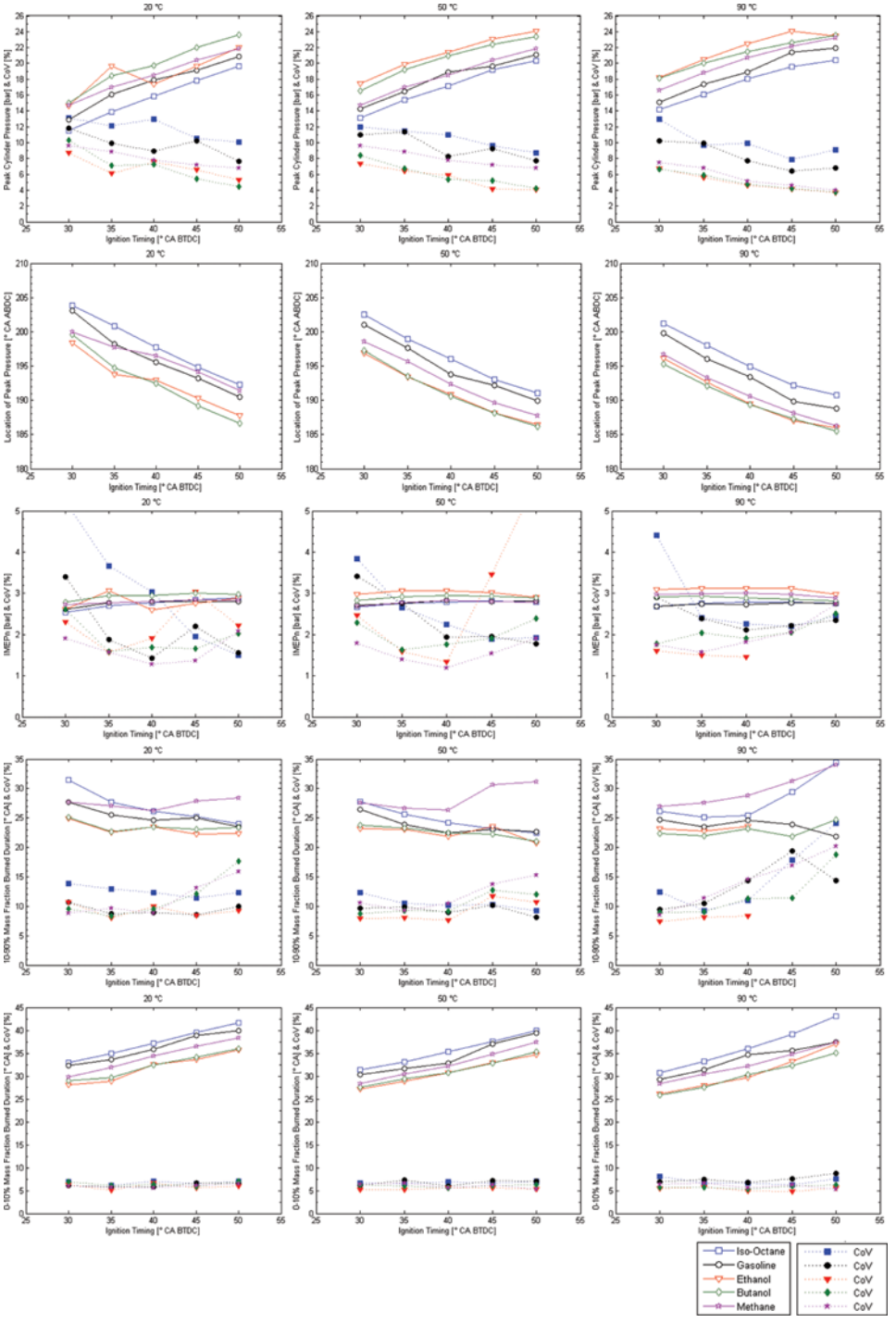

Figure 10 Combustion performance with triple injection strategy at 20°C, 50°C, and 90°C; all fuels ($\lambda = 1.0$). (Figure is provided in color online.)

At 50°C, butanol showed clear signs of approaching ethanol's P_{max}, and at 90°C the performance of the two alcohols was very similar. The COV_{Pmax} was also very similar for ethanol and butanol throughout 50–90°C, typically about 4–7% depending on spark advance. Gasoline and methane remained quite close over the full range of temperatures and spark advances, with greatest similarity at the higher spark advances when the engine was cold and at the lower spark advances when the engine's set temperature was 50–90°C. *Iso*-octane remained clearly isolated throughout most tested conditions, except with the large spark advances at 50–90°C. At the larger spark advances of 40°–50°CA the COV_{Pmax} of both alcohols was quite similar to that of methane (4–6%), and the P_{max} of methane was lower than the alcohols' by only 0.5–1.5 bar. It is interesting to point out that the differences in spray break-up and evaporation at low temperatures for the two alcohol fuels observed in Serras-Pereira et al. (2008) and Aleiferis and van Romunde (2013) did not really appear to impede those fuels from achieving similar or better performance than the hydrocarbons.

With respect to IMEP, it was clear that the ignition timing did not impact significantly the useful work done by the engine. At the cold-start representative engine condition of 20°C, all fuels showed a preference for more advanced ignition timing, between 40°–45°CA BTDC; this also produced the lowest levels of COV_{IMEP} (typically 1.5–2.5%). Specifically, methane and gasoline produced the lowest COV_{IMEP}, while butanol produced generally the highest COV_{IMEP} followed by *iso*-octane and ethanol. Based on the atomization processes of the fuels described in Serras-Pereira et al. (2008) and Aleiferis and van Romunde (2013), it may be speculated that the differences in the mixture preparation quality did contribute to the observed levels of COV_{IMEP}, especially at the cold engine conditions. This note is consistent with the data at 90°C, where all fuels produced similar levels of COV_{IMEP}, ~2%, with ethanol at the higher end and *iso*-octane at the lower end of variability, particularly at the higher spark advances. It should also be noted that the fuel injection durations were much longer for the alcohols, reducing their effective time for evaporation and the potential for the formation of a homogeneous concentration field.

At the lean condition of $\lambda = 1.2$ in Figure 9, the levels of IMEP dropped by about 35% for most fuels in comparison to $\lambda = 1.0$. Overall, the alcohols were more robust to changes in fueling in comparison to the liquid hydrocarbons. The COV_{IMEP} increased to levels of beyond 10–20% for *iso*-octane at 20–50°C, but the alcohols did not exceed 8% even at their worst points. Gasoline lied lower than *iso*-octane but higher than both alcohols in terms of COV_{IMEP}. Methane maintained the lowest levels of COV_{IMEP} and COV_{Pmax} at lean conditions in comparison to all the other fuels. The plots of the phasing of P_{max} also clearly reflected the different behaviors among fuels. In contrast to stoichiometric conditions, lean *iso*-octane and gasoline showed a nonlinear relationship with the spark advance, while the alcohols and methane maintained a monotonic relationship of lower gradient to that at $\lambda = 1.0$. Overall, ignition timing had to be advanced by 10–15°CA in order to achieve maximum IMEP with minimum COV_{IMEP}.

Mass fraction burned and combustion duration. In the initial stages of combustion, the 0–10% MFB period ($\chi_{b10\%}$) showed that ethanol had consistently the fastest burning rate throughout the range of spark advances tested. The early

burning period for methane was nearly identical in duration to ethanol's but the levels of COV$\chi_{b10\%}$ were slightly lower for methane (~1%). Butanol was the third fastest fuel for the initial burning period but produced the highest COV$\chi_{b10\%}$ at 20°C, ~7.5% compared to ~6% for methane (most probably due to fuel films on the walls from spray impingement that led to a large degree of stratification). Gasoline and *iso*-octane had the slowest initial burn periods, with *iso*-octane ~20% slower than the fastest fuels, despite its AFR at the spark-plug location being on the rich side as will be discussed in the next section. At 50°C the differences in the 0–10% MFB duration reduced noticeably, with the largest difference now only 12–14% between *iso*-octane and ethanol. The levels of variability also reduced, in particular for the alcohols. Ethanol's behavior may be a result of the local AFR at the spark plug location that was consistently close to stoichiometric or slightly rich. Butanol produced a very similar 0–10% MFB duration at 50°C compared to both ethanol and methane. At 90°C these trends were further emphasized with ethanol, butanol, and methane tightly grouped as the faster fuels and gasoline and *iso*-octane clearly slower across the range of spark timings. It should be noted that the 0–10% MFB duration for methane did not change significantly with increasing engine temperature but was clearly reduced for the liquid fuels, indicating that temperature effects had specific bearing on the combustion quality of the liquid fuels. The latter can be associated with better fuel mixing and higher laminar flame speeds due to higher temperature at ignition timing.

The main combustion stage, described by the 10–90% MFB ($\chi_{b10-90\%}$) showed how similarities between fuels in the early stages of combustion could disappear by the later stages. For example, methane was one of the fastest early burning fuels, but showed a slower main period of combustion that increased its $\chi_{b10-90\%}$ duration. The liquid fuels on the other hand showed more consistency between early stage combustion duration and main stage combustion duration. The main stage of combustion at 20°C was clearly fastest for ethanol, with butanol and gasoline very similar and *iso*-octane and methane the slowest (depending on spark advance). At 50°C, the $\chi_{b10-90\%}$ duration of butanol, gasoline, and *iso*-octane were nearly identical for most ignition timings, while ethanol and methane remained fastest and slowest, respectively, and were both negatively affected by large spark advances. At 90°C, butanol exhibited generally faster $\chi_{b10-90\%}$, followed by overlapping ethanol and gasoline, then *iso*-octane and finally methane. *Iso*-octane and methane were particularly sensitive to larger spark advances at high temperatures, which increased their burn durations and levels of COV. The results appeared to suggest that fuels which were likely to experience the slowest evaporation rates overall, produced faster main combustion periods. Whether this resulted from the presence of microsized droplets in the charge that increased the burn rate (e.g., by enhancing flame cellularity) is not explicitly known under the range of conditions studied, but it is a clear possibility for the worst atomized fuels. It is interesting to note, however, that the recent work by Szwaja and Naber (2010) on butanol combustion in an SI engine with PFI, found that pure butanol was always faster than gasoline at the fully warm engine conditions they used.

More to the point made about the effect of spark advance on IMEP earlier, there was also clear trend in the COV$\chi_{b10-90\%}$ for all fuels in terms of optimum spark timing at different engine temperatures. At 20°C, the fastest and most repeatable combustion duration was achieved with 40°CA spark advance, but this was seen

to migrate towards more retarded timings at higher temperatures, 35°CA at 50°C and 30°CA at 90°C; these advances also coincided with the lowest levels of COV_{IMEP}. Given the relatively flat IMEP relationship with spark advance over most engine temperatures, it appeared that there was limited room for using fuel-specific timings to achieve higher work output, but it was clear that while retarded ignition shortened the early burn period (as a result of higher in-cylinder pressures and temperatures at ignition timing), the benefit did not necessarily extend into the main combustion stage, which was generally slower except under fully warmed-up engine conditions. Overall, a spark advance of 35°CA was a relatively good compromise as the representation of the "minimum spark advance for best torque" (MBT) across all fuels at engine temperatures 50–90°C for $\lambda = 1.0$. For lean fueling in Figure 9, the early burning period of 0–10% MB was typically prolonged by about 5–7°CA for all fuels throughout the full range of spark advances, with gasoline and *iso*-octane affected the most.

Careful consideration of the fuels' laminar burning velocities is essential for interpretation of the MFB data. Such data are available from various sources for typical fuels, including butanol recently, but most have been taken at various "engine-like" conditions of temperature and pressure; hence it is not straightforward to carry out direct comparisons among fuels, especially if the effect of residual gas needs to be taken into account as well (e.g., see Beeckmann et al., 2009, 2010; Bradley et al., 1998, 2009; Gu et al., 2000, 2009; Jerzembeck et al., 2009). A thorough literature review of such data is currently being undertaken by the current authors, and the results will be unified and presented in a forthcoming publication. In general, at conditions of $\lambda = 1.0$ at about 5 bar and 350 K without residuals, *iso*-octane's laminar flame speed is slower than gasoline's by ~6%, methane's is slower than *iso*-octane's by ~10%, while ethanol's is very similar to gasoline's and butanol's is ~7% greater than ethanol's. At lean conditions of about $\lambda = 1.2$, the main hierarchy among these fuels holds, but the differences become too small to be very useful. With regard to turbulent burning velocities, the picture is even less clear, with detailed published data on butanol missing (Bradley et al., 2011; Lawes et al., 2005; Sheppard and Lawes, 2009). Considering that methane has the lowest laminar burning velocity, but it was found to perform similarly in terms of 0–10% MFB to ethanol, and for butanol, whose laminar burning velocities are quite higher, an analysis of the effect of charge cooling was undertaken. It was found that close to ignition timing (35–60°CA BTDC), the in-cylinder pressure was higher with methane than those of the liquid fuels throughout the range of engine temperatures, despite not adjusting the engine load for methane to account for air displacement. Among the liquid fuels, there was very little difference, however. Specifically, methane's pressure at ignition timing was ~0.2 bar higher than those of the liquid fuels at 90°C and ~0.1 bar at 20°C. This translated to ~25 K higher temperature at ignition timing for methane, which, when combined with consistent homogeneous fueling, can account for its observed overlapping with the alcohols in terms of the duration of 0–10% MFB. The differences in pressure among all liquid fuels were typically smaller than ~0.05 bar and in terms of temperature smaller than ~10 K. Given the higher latent heat of evaporation of both alcohols relative to *iso*-octane and gasoline, one might have expected ethanol in particular to have exhibited much higher levels of charge cooling overall, hence quite lower temperature and pressure at ignition timing in

comparison to the hydrocarbons. Analysis of data from evaporation modeling and wall heat flux measurements with the exact same liquid fuels by Aleiferis et al. (2011), and from charge cooling measurements with various oxygenated blends using a cold wire resistance thermometer by Price et al. (2007) in an engine of same nominal geometry to that of the current study, indicated that the higher levels of charge cooling during injection with alcohol fuels can result in gradual reduction in the evaporation rate overall because the latter can be limited by fuel saturation due to the higher mass injected and/or by diffusion and mixing. Specifically, the overall effect of saturation was a temperature difference between gasoline and ethanol at the spark-plug location at ignition timing of only ~8 K (Price et al., 2007). Saturation in temperature drop during injection has also been measured optically by Beyrau et al. (2006) with *iso*-octane fuel.

Mixture Stratification

Analysis of the combustion performance matrix for the triple-injection strategy in Figure 10 shows that the hierarchy seen among fuels in Figure 8 (when single-injection was employed) has been maintained. However, it interesting to note that ethanol and butanol seem to have benefited from this new strategy because the levels of IMEP marginally increased, while *iso*-octane and gasoline saw a marginal decrease. In terms of combustion stability though, the effect was clearly negative for most conditions, with higher COV levels recorded typically throughout. *Iso*-octane and gasoline were again the worst affected fuels, but ethanol and to some extent butanol seem to have benefited especially at the lower temperatures and lower spark advances. This highlights the effect of better atomization and mixing for the two alcohols when introduced into the cylinder with split injection events.

In order to study the differences in mixture stratification among fuels and injection strategies, the FFID data were converted to AFR (λ) according to the molar ratios of the respective stoichiometric chemical equation for each fuel. The results in Figure 11 showed that differences in the gaseous mole fractions between fuels did exist. Reference to gaseous mole fraction is important here, because it was found that there were some clear signs of a "wetted" spark-electrode and pent-roof from

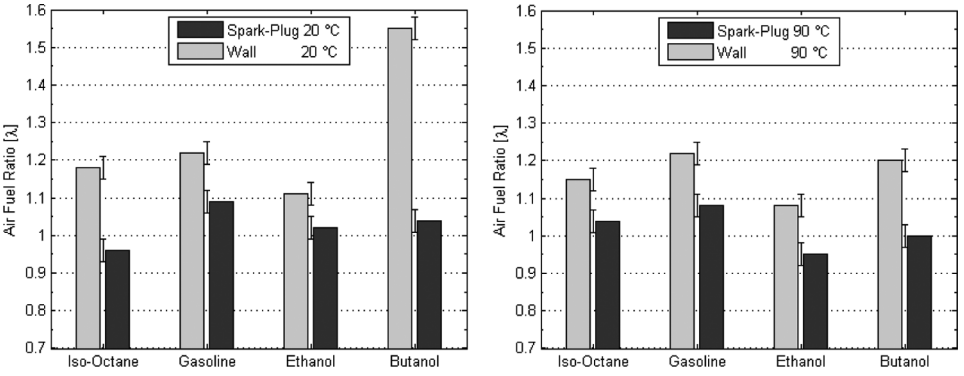

Figure 11 AFR at the spark-plug location and at the cylinder wall.

the injection event, even under firing conditions, especially at 20°C. The presence of liquid fuel was likely to be different for each fuel, but this is not measured by the FFID instrument because it only responds to fuel vapor in the vicinity of the sampling probe. The results should therefore be studied within this context and interpreted accordingly. Differences were seen between the data obtained at the spark-plug location and those sampled at the pent-roof wall. The degree of this stratification was generally higher for cold engine conditions. At 20°C, the value of λ was in the range 0.96–1.09 at the spark plug location, with gasoline exhibiting the largest and *iso*-octane the lowest value; ethanol and butanol were close to 1.02 and 1.04, respectively. Specifically for butanol at 20°C, the wall region was found to be considerably leaner in vapor concentration than the center of the chamber, most possibly because of the presence of significant unevaporated liquid fuel on the cylinder walls from spray wall impingement; this agrees with the spray impingements study of Aleiferis et al. (2011). Ethanol showed the lowest degree of stratification with a difference in λ of $\sim$0.08. At 90°C, gasoline showed a very similar degree of stratification to that at 20°C, while *iso*-octane's degree of stratification was lower, i.e., the iso-octane's concentration field was more homogeneous than at 20°C. Butanol showed an almost perfect $\lambda = 1.0$ value at the spark plug location, with a much lower degree of stratification than at 20°C, as the value of butanol's λ at the wall did not exceed 1.2. Ethanol exhibited a richer mixture than stoichiometric at the spark-plug location ($\lambda = 0.96$), and this may explain the consistently fast burning behavior of ethanol throughout most testing conditions.

The FFID results obtained were compared to PLIF measurements carried out by Williams et al. (2008) in an identical engine at the same operating conditions. In order for the PLIF measurements of fuel distribution to represent those of a real gasoline fuel, a nonfluorescing multicomponent "model"-fuel comprising low, medium, and high boiling point constituents was chosen to co-evaporate with one of three tracers: namely, acetone, toluene, and 1,2,4-trimethylbenzene. The model fuel exhibited a volatility curve very similar to the gasoline used in the current study. This PLIF fuel was also tested at University College London in a quiescent chamber, and its spray formation was shown to behave similarly to standard gasoline over the range of pressures and temperatures relevant for DISI operation (van Romunde and Aleiferis, 2009). The PLIF results showed that for all early injection strategies up to 240°CA ATDC (or 120°CA BTDC), the fuel was found to largely follow the bulk tumble motion in the cylinder from a few tens of degrees after the end of injection. Mean and standard deviation values of equivalence ratio were evaluated from 32 cycles in the area close to the spark plug. These can be compared to the values obtained for gasoline using the FFID in the current work. At ignition timing, between 30°–40° BTDC, the FFID values of $\lambda = 1.08$ obtained by the current authors for gasoline (Figure 11) were in closest agreement to those obtained for toluene using PLIF, with a value of $\lambda = 0.98$ at 40°CA BTDC. Cyclic variability in the FFID plateau signal levels at the spark-plug had a COV of $\sim$10% compared to $\sim$20% for PLIF values. However, the local mixture in-homogeneity was calculated to be $\leq$10% on a scale above 350 μm at ignition, in closer agreement with the more robust FFID values, whose absolute uncertainties were very low, demonstrated by gaseous methane fueling which produced a COV of $<$1% in the FFID signal plateau values. The single shot PLIF images also showed evidence of droplets, with a

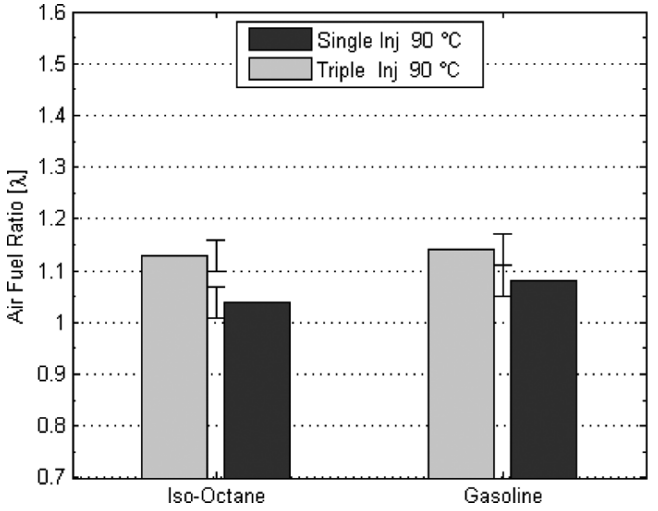

Figure 12 AFR at the spark-plug location with single and triple injection strategies.

particularly large one appearing in one of the images; this droplet was reported to have originated from the injector tip, and indeed, it will be shown in later sections of this article, that localized regions of high flame chemiluminescence emanating from directly under the injector were also imaged, possibly from trapped fuel inside the outer nozzle section of the injector. The single shot PLIF images certainly suggested that the mixture field was significantly heterogeneous, even with early injection in the intake stroke. In order to check this hypothesis, the triple injection tests were also repeated with a FFID sampling probe at the spark-plug. These results are shown in Figure 12. Indeed a triple injection strategy produced marginally leaner AFR for both *iso*-octane and gasoline.

Previous work with single and triple injection strategies using combustion imaging during the early stages of combustion with the "standard" quartz optical showed that the triple injection flames also suggested a leaner fuel concentration at the spark plug location at ignition timing than the single injection strategy. Lower

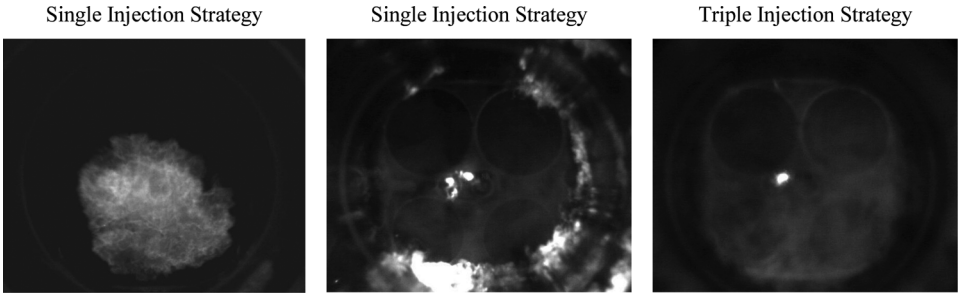

Figure 13 Examples of late burning period for three instantaneous cycles using full-bore optical piston with single injection (left) and triple injection (right) strategy, 80°CA after ignition timing.

luminosity and more "circular" flame growth on a macroscale also resonated with traditional stoichiometric PFI charge preparation combustion systems than DI systems. For triple injection, the absence of a distribution of bright localized luminous spots in the flame (seen for single-injection) also suggested minimal diffusion burning phenomena and soot production. In the current study, imaging using the full-bore optical piston allowed the combustion process to be visualized until the flame reached the cylinder walls. Figure 13 shows a flame at 28°CA after ignition timing (AIT), i.e., after the typical timing of 25°CA AIT. With this flame, "masking" effects would have been introduced by the "standard" quartz crown (Serras-Pereira et al., 2007, 2008), and two images of combustion completion at 80°CA after ignition timing, with single and triple injection strategies (45°CA after compression TDC). Those late combustion stages with single injection were clearly observed to produce more diffusion burning around the cylinder walls from the "out-gassing" of crevice volumes and likely presence of wall-films when compared to triple injection. This is a straight indication of the effect of liquid fuel impingement on the cylinder's liner observed with single injection, and it is expected to influence the emissions characteristics of this strategy. The levels of late diffusion burning shown for single injection in Figure 13 were representative of at least 50% of the imaged cycles, whereas no single imaged cycle ever produced such luminous levels of late burning with triple injection over a series of 100 consecutive cycles. The "diffusion" burning regions observed for both the single and triple injection strategies in the center of the chamber were found to stem from the injector tip; similar observations were made with the single-injection strategy employed in the PLIF study of Williams et al. (2008).

SUMMARY AND CONCLUSIONS

This article presented results from a detailed study of combustion of gasoline, *iso*-octane, ethanol, and butanol fuels in a DISI engine for various engine temperatures. The fuels were injected from a multihole injector located centrally in the combustion chamber, in close proximity to the spark plug. Methane was also employed by injecting it into the inlet plenum of the engine to provide a benchmark case for a well-mixed "homogeneous" mixture preparation. Several key operating conditions were examined, e.g., stoichiometric ($\lambda = 1$) and lean ($\lambda = 1.2$) mixtures, spar advances, and injection strategies (single and "split" triple per cycle). In-cylinder gas sampling at the spark-plug location and at a location on the pent-roof wall was also carried out with a fast flame ionization detector, in order to obtain the equivalence ratio and study possible stratification in the mixture field for all liquid fuels. The analysis was complemented by imaging the combustion at completion using a full-bore optical piston to study the effect of injection strategy on late burning due to "pool" fires on the cylinder walls from spray wall impingement. The main conclusions of this study can be summarized as follows:

- Combustion with single injection strategy was fastest for ethanol throughout the 20–90°C engine coolant temperature range, but butanol and methane flames were just as fast at 90°C. *Iso*-octane was the slowest by some margin at all temperatures, while gasoline flame development fell in between *iso*-octane and the

alcohols. However, butanol was more difficult, indeed, to ignite at cold engine conditions with higher degree of variability in IMEP and duration of mass fraction burned in the early stage of combustion 0–10% and 10–90%. Overall, a spark advance of 35°CA was a relatively good compromise as the representation of the minimum spark advance for best torque across all fuels at engine temperatures 50–90°C for $\lambda = 1.0$.

- The AFR measurements at the spark-plug and the cylinder walls indicated a certain degree of stratification for all fuels. At 20°C, the value of λ was in the range 0.96–1.09 at the spark plug location, with gasoline exhibiting the largest and *iso*-octane the lowest value; ethanol and butanol were close at 1.02 and 1.04, respectively. For butanol, the wall region was found to be considerably leaner in vapor concentration than the center of the chamber, most possibly because of the presence of significant unevaporated liquid fuel on the cylinder walls from spray wall impingement. Ethanol showed the lowest degree of stratification with a difference in λ of $\sim$0.08. At 90°C, gasoline showed a very similar degree of stratification to that at 20°C, while *iso*-octane's degree of stratification was lower (more homogeneous) than at 20°C. Butanol showed an almost perfect $\lambda = 1.0$ value at the spark plug location, with a much lower degree of stratification than at 20°C (the value of λ at the wall did not exceed 1.2). Ethanol exhibited a richer mixture than stoichiometric at the spark-plug location ($\lambda = 0.96$), and this may explain the consistently fast burning behavior of ethanol throughout most testing conditions.
- The alcohols were more robust to changes in fueling in comparison to the liquid hydrocarbons. Specifically, the early burning period of 0–10% mass fraction burned was typically prolonged by about 5–7°CA for all fuels throughout the full range of spark advances, with gasoline and *iso*-octane affected the most. The levels of IMEP dropped by about 35% for most fuels in comparison to $\lambda = 1.0$. The COV_{IMEP} increased to levels of beyond 10–20% for *iso*-octane at 20–50°C, but ethanol and butanol did not exceed 8% even at their worst points; gasoline performed between *iso*-octane and both alcohols. Methane maintained the lowest levels of COV_{IMEP} at lean conditions. Overall, ignition timing had to be advanced by 10–15°CA for all fuels in order to achieve maximum IMEP with minimum COV_{IMEP}.
- Considering that methane has the lowest laminar burning velocity, but it was found to perform similarly in terms of 0–10% MFB to ethanol and butanol whose laminar burning velocities are quite higher, an analysis of the effect of charge cooling was undertaken. It was found that close to ignition timing, the in-cylinder pressure was higher with methane than with the liquid fuels, despite not adjusting the engine load for methane to account for air displacement. Among the liquid fuels, there was very little difference. Specifically, methane's pressure at ignition timing was $\sim$0.2 bar higher than those of the liquid fuels at 90°C and $\sim$0.1 bar at 20°C. This translated to $\sim$25 K higher temperature at ignition timing for methane, which when combined with consistent homogeneous fueling, could account for its similarity to the behavior of alcohols in terms of the duration of 0–10% mass fraction burned. The differences in pressure among all liquid fuels were typically smaller than $\sim$0.05 bar and in terms of temperature smaller than $\sim$10 K.

- Triple injection had a small but noticeable impact on the combustion performance of the different fuels with $\lambda = 1.0$. IMEP marginally increased for the alcohols and marginally decreased for *iso*-octane and gasoline. The effect on combustion stability, though, was clearly negative for most conditions, with higher COV typically recorded throughout. *Iso*-octane and gasoline were again the worst affected fuels, but ethanol and to some extent butanol benefited, especially at the lower temperatures and lower spark advances. This highlights the effect of better atomization and mixing for the two alcohols when introduced into the cylinder with split injection events. Triple injection produced less stratification in mixture concentration, with a generally leaner mixture at the spark plug than single injection.
- Images of combustion completion with single- and triple-injection strategies showed much less luminous late burning for the triple-injection strategy, typically synonymous with lower levels of soot production.

Our current work is focused on analysis of in-cylinder flame images with all fuels in order to derive rates of flame kernel growth and motion. Linking those to carefully categorized laminar and turbulent burning velocities, as well as to traditional combustion diagrams, will provide further insights into the effects observed in the present article.

ACKNOWLEDGMENTS

The authors would like to thank Jaguar Cars for financial and technical support, as well as Shell Global Solutions (UK) for fuel supplies. Technical support by Mark Peckham (Cambustion Ltd.) is gratefully acknowledged.

NOMENCLATURE

λ	air to fuel excess ratio ($=AFR/AFR_{stoich}$)
P_{max}	peak in-cylinder pressure
χ_b	mass fraction burned (MFB)
$\chi_{b10\%}$	duration of 0–10% MFB
$\chi_{b10–90\%}$	duration of 10–90% MFB

REFERENCES

Alasfour, F.N. 1997. Butanol—a single cylinder engine study: engine performance. *Int. J. Energy Res.*, **21**, 21–30.

Aleiferis, P.G., Malcolm, J.S., Todd, A.R., Cairns, A., and Hoffmann, H. 2008. An optical study of spray development and combustion of ethanol, iso-octane and gasoline blends in a DISI engine. SAE Paper 2008-01-0073.

Aleiferis, P.G., Serras-Pereira, J., Augoye, A., Davies, T.J., Cracknell, R.F., and Richardson, D. 2010. Effect of fuel temperature on in-nozzle cavitation and spray formation of liquid hydrocarbons and alcohols from a real-size optical injector for direct-injection spark-ignition engines. *Int. J. Heat Mass Transfer*, **53**, 4588–4606.

Aleiferis, P.G., Serras-Pereira, J., and Richardson, D. 2011. Imaging and heat flux measurements of impinging sprays of liquid hydrocarbons and alcohols in a direct-injection spark-ignition engine. *Fuel*, **91**, 264–297.

Aleiferis, P.G., Serras-Pereira, J., van Romunde, Z., Caine, J., and Wirth, M. 2010. Mechanisms of spray formation and combustion from a multi-hole injector with E85 and gasoline. *Combust. Flame*, **157**, 735–756.

Aleiferis, P.G., and van Romunde, Z. 2013. An analysis of spray development with ethanol, butanol, iso-octane, n-pentane and gasoline fuels from a multi-hole injector under hot fuel conditions. *Fuel*, **105**, 143–168.

Al-Farayedhi, A.M., Al-Dawood, P., and Gandhidasan, P. 2004. Experimental investigation of SI engine performance using oxygenated fuel. *J. Eng. Gas Turbines Power*, **126**, 178–191.

Ball, J.K., Raine, R.R., and Stone, C.R. 1998. Combustion analysis and cycle-by-cycle variations in spark ignition engine combustion—part 1: An evaluation of combustion analysis routines by reference to model data. *Proc. IMechE, Part D*, **212**, 381–399.

Beeckmann, J., Kruse, S., and Peters, N. 2010. Effect of ethanol and n-butanol on standard gasoline regarding laminar burning velocities. SAE Paper 2010-01-1452.

Beeckmann, J., Rohl, O., and Peters, N. 2009. Numerical and experimental investigation of laminar burning velocities of iso-octane, ethanol and n-butanol. SAE Paper 2009-01 -2784.

Beyrau, F., Weikl, M.C., Schmitz, I., Seeger, T., and Leipertz, A. 2006. Locally resolved investigation of the vaporization of GDI sprays applying different laser techniques. *Atomization Sprays*, **16**, 319–330.

Bradley, D., Hicks, M., Lawes, M., Sheppard, C.G.W., and Woolley, R. 1998. The measurement of laminar burning velocities and Markstein numbers for iso-octane–air and iso-octane–n-heptane–air mixtures at elevated temperatures and pressures in an explosion bomb. *Combust. Flame*, **115**, 126–144.

Bradley, D., Lawes, M., and Mansour, M.S. 2009. Explosion bomb measurements of ethanol-air laminar gaseous flame characteristics at pressures up to 1.4 MPa. *Combust. Flame*, **156**, 1462–1470.

Bradley, D., Lawes, M., and Mansour, M.S. 2011. Correlation of turbulent burning velocities of ethanol-air, measured in a fan-stirred bomb up to 1.2 MPa. *Combust. Flame*, **158**, 123–138.

Brewster, S. 2007. Initial development of a turbo-charged direct injection E100 combustion system. SAE Paper 2007-01-3625.

Brinkman, N.D. 1981. Ethanol fuel—a single cylinder engine study of efficiency and exhaust emissions. SAE Paper 810345.

Brunt, M.F., and Emtage, A.L. 1996. Evaluation of IMEP routines and analysis errors. SAE Paper 960609.

Cairns, A., Stansfield, P., Fraser, N., Blaxill, H., Gold, M., Rogerson, J., and Goodfellow, C. 2009. A study of gasoline-alcohol blended fuels in an advanced turbocharged DISI Engine. SAE Paper 2009-01-0138.

Cheng, W.K., Summers, T., and Collings, N. 1998. The fast-response flame ionisation detector. *Prog. Energy Combust. Sci.*, **24**, 89–124.

Davis, G.W., and Heil, E.T. 2000. The development and performance of a high blend ethanol fuelled vehicle. SAE Paper 2000-01-1602.

Dec, J.E., Davisson, M.L., Sjöberg, M., Leif, R.N., and Hwang, W. 2008. Detailed HCCI exhaust speciation and the sources of hydrocarbon and oxygenated hydrocarbon emissions. SAE Paper 2008-01-0053.

Gautam, M., and Martin, D.W. 2000. Combustion characteristics of higher alcohol/gasoline blends. *Proc. IMechE, Part A*, **214**, 497–511.

Gautam, M., Martin, D.W., and Carder, D. 2000. Emissions characteristics of higher alcohol/gasoline blends. *Proc. IMechE, Part A*, **214**, 165–182.

Gu, X., Huang, Z., Li, Q., and Chenglong, T. 2009. Measurements of laminar burning velocities and markestein lengths of n-butanol-air premixed mixtures at elevated temperatures and pressures. *Energy Fuels*, **23**, 4900–4907.

Gu, X.J., Haq, M.Z., Lawes, M., and Wooley, R. 2000. Laminar burning velocity and Markstein lengths of methane-air mixtures. *Combust. Flame*, **121**, 41–58.

Guerrieri, D.A., Caffrey, P.J., and Rao, V. 1995. Investigation into the vehicle exhaust emissions of high percentage ethanol blends. SAE Paper 950777.

Gupta, R.B., and Demirbas, A. 2010. *Gasoline, Diesel and Ethanol Biofuels from Grasses and Plants*, Cambridge University Press, Cambridge, UK.

Jerzembeck, S., Peters, N., Pepiot-Desjardins, P., and Pitsch, H. 2009. Laminar burning velocities at high pressure for primary reference fuels and gasoline: Experimental and numerical investigation. *Combust. Flame*, **156**, 292–301.

Kapus, P.E., Fuerhapter, Fuchs, H., and Fraidl, G.K. 2007. Ethanol direct injection on turbocharged SI engines—potentials and challenges. SAE Paper 2007-01-1408.

Lawes, M., Ormsby, M.P., Sheppard, C.G.W., and Woolley, R. 2005. Variation of turbulent burning rate of methane, methanol, and iso-octane air mixtures with equivalence ratio at elevated pressure. *Combust. Sci. Technol.*, **177**, 1273–1289.

Lotus Engine Simulation Software, http://www.lesoft.co.uk/index.html, 2010.

Ma, H., Marshall, S., Stevens, R., and Stone, R. 2007. Full-bore crank-angle resolved imaging of combustion in a four-stroke gasoline direct injection engine. *Proc. IMechE, Part D*, **221**, 1305–1320.

Martinez, F.A., and Ganji, A.R. 2006. Performance and exhaust emissions of a single-cylinder utility engine using ethanol fuel. SAE Paper 2006-32-0078.

Nakata, K., Utsumi, S., Ota, A., Kawatake, K., Kawai, T., and Tsunooka, T. 2006. The effect of ethanol on a spark ignition engine. SAE Paper 2006-01-3380.

Owen, K., and Coley, T. 1995. *Automotive Fuels Reference Book*, Society of Automotive Engineers, Warrendale, PA.

Perry, R.H., and Green, D.W. 1997. *Perry's Chemical Engineers' Handbook*, 7th ed., McGraw-Hill, New York.

Poling, B.E., Prausnitz, J.M., and O'Connell, J.P. 2001. *The Properties of Gases and Liquids*, 5th ed., McGraw-Hill, New York.

Price, P., Twiney, B., Stone, R., Kar, K., and Walmsley, H. 2007. Particulate and hydrocarbon emissions from a spray guided direct injection spark ignition engine with oxygenate fuel blends. SAE Paper 2007-01-0472.

Sandiquist, H., Karlsson, M., and Denbratt, I. 2001. Influence of ethanol content in gasoline on speciated emissions from a direct-injection stratified charge SI engine. SAE Paper 2001-01-1206.

Scharlab, S.L. 2011a. Data Sheet 1-Butanol, HPLC grade.

Scharlab S.L. 2011b. Data Sheet 2,2,4-Trimethylpentane, anhydrous.

Scharlab, S.L. 2011c. Data Sheet Ethanol absolute, analytical grade, ACS.

Serras-Pereira, J., Aleiferis, P.G., Richardson, D., and Wallace, S. 2007. Mixture formation and combustion variability in a spray-guided DISI engine. SAE Paper 2007-01-4033.

Serras-Pereira, J., Aleiferis, P.G., Richardson, D., and Wallace, S. 2008. Characteristics of ethanol, butanol, iso-octane and gasoline sprays and combustion from a multi-hole injector in a DISI engine. SAE Paper 2008-01-1591.

Shell Global Solutions (UK). 2005.

Sheppard, C.G.W., and Lawes, M. 2009. Personal communication.

Smith, J.D., and Sick, V. 2007. The prospects of using alcohol-based fuels in stratified-charge spark-ignition engines. SAE Paper 2007-01-4034.

Stone, C.R., and Green-Armytage, D.I. 1987. Comparison of methods for the calculation of mass fraction burnt from engine pressure-time diagrams. *Proc. IMechE, Part D*, **201**, 61–67.

Szwaja, S., and Naber, J.D. 2010. Combustion of n-butanol in a spark-ignition engine. *Fuel*, **89**, 1331–1748.

Topgül, T., Yücesu, H.S., Cinar, C., and Koca, A. 2006. The effects of ethanol-unleaded gasoline blends and ignition timing on engine performance and exhaust emissions. *Renewable Energy*, **31**, 2534–2542.

van Romunde, Z., and Aleiferis, P.G. 2009. Effect of operating conditions and fuel volatility on development and variability of sprays from gasoline direct-injection multi-hole injectors. *Atomization Sprays*, **19**, 207–234.

van Romunde, Z., Aleiferis, P.G., Cracknell, R.F., and Walmsley, H.L. 2007. Effect of fuel properties on spray development from a multi-hole DISI engine injector. SAE Paper 2007-01-4032.

Wallner, T. 2011. Correlation between speciated hydrocarbon emissions and flame ionization detector response for gasoline/alcohol blends. *J. Eng. Gas Turbines Power*, **133**, 082801-1-082801-8.

Wallner, T., and Frazee, R. 2010. Study of regulated and non-regulated emissions from combustion of gasoline, alcohol fuels and their blends in a DI-SI engine. SAE Paper 2010-01-1571.

Wallner, T., Miers, S.A., and Mconnell, S. 2009. A comparison of ethanol and butanol as oxygenates using a direct-injection, spark-ignition engine. *J. Eng. Gas Turbines Power*, **131**, 032802-1-032802-9.

Williams, B., Ewart, P., Stone, R., Ma, H., Walmsley, H., Cracknell, R., Stevens, R., Richardson, D., Qiao, J., and Wallace, S. 2008. Multi-component quantitative PLIF: Robust engineering measurements of cyclic variation in a firing spray-guided gasoline direct injection engine. SAE Paper 2008-01-1073.

Yaws, C.L. 2003. *yaws' Handbook of Thermodynamic and Physical Properties of Chemical Compounds*, Knovel, New York.

Zhu, G., Stuecken, T., Schock, H., Yang, X., Hung, D., and Fedewa, A. 2008. Combustion characteristics of a single-cylinder engine equipped with gasoline and ethanol dual-fuel systems. SAE Paper 2008-01-1767.